Journal of Functional Foods 92 (2022) 105066

Contents lists available at ScienceDirect

Journal of Functional Foods

journal homepage: www.elsevier.com/locate/jff

Design and characterization of Ca-Fe(III) pyrophosphate salts with tunable pH-dependent solubility for dual-fortification of foods

Neshat Moslehi [a,1], Judith Bijlsma [b,1], Wouter J.C. de Bruijn [b], Krassimir P. Velikov [c,d,e], Jean-Paul Vincken [b], Willem K. Kegel [a,*]

[a] Van 't Hoff Laboratory for Physical and Colloid Chemistry, Debye Institute for Nanomaterials Science, Utrecht University, Padualaan 8, 3584 CH Utrecht, the Netherlands
[b] Laboratory of Food Chemistry, Wageningen University & Research, Bornse Weilanden 9, P.O. Box 17, 6700 AA Wageningen, the Netherlands
[c] Unilever Innovation Centre Wageningen, Bronland 14, 6708 WH Wageningen, the Netherlands
[d] Soft Condensed Matter, Debye Institute for Nanomaterials Science, Utrecht University, Princetonplein 5, 3584 CC Utrecht, the Netherlands
[e] Institute of Physics, University of Amsterdam, Science Park 904, 1098 XH Amsterdam, the Netherlands

ARTICLE INFO

Keywords:
Mixed mineral salt
Calcium-iron (III) pyrophosphate salt
Ferric pyrophosphate
Food fortification
Iron supplementation
Dissolution behavior

ABSTRACT

Food-fortification using poorly water-soluble mineral-containing compounds is a common approach to deliver iron. However, it comes with the challenge of ensuring iron bio-accessibility and limiting iron-phenolic interactions that can change organoleptic properties. Mixed Ca-Fe(III) pyrophosphate salts with the general formula $Ca_{2(1-x)}Fe_{4x}(P_2O_7)_{(1+2x)}$ were designed as a system for simultaneous delivery of iron and calcium. The salts were synthesized via a co-precipitation method and characterized by TEM-EDX, XRD, and FT-IR. All mixed salts with $0.14 \leq x \leq 0.35$ yielded homogenous amorphous particles. The iron dissolution from these mixed salts showed a fourfold increase at gastric pH compared to Fe(III) pyrophosphate. In the food-relevant pH range, the salts with $x \leq 0.15$ showed up to an eight-fold decrease in iron solubility. Despite this, reactivity of the mixed salts in tea was similar to that of FePP. Our results indicate that these mixed salts are potential dual-fortificants with tunable iron content and solubility.

1. Introduction

Micronutrient fortification of foods can effectively overcome mineral and vitamin deficiencies (Díaz et al., 2003; Saha & Roy, 2020). Among minerals, particularly iron receives significant attention since one-quarter of the world's population is affected by iron deficiency anemia (Allen et al., 2006). However, iron is a challenging mineral to introduce to food products due to the high reactivity of 'free' iron ions (Habeych et al., 2016). Iron compounds are highly reactive with food products because of the complexation and oxidation of iron with phenolics that are abundant in plants and vegetables (Ashwin et al., 2021; Bijlsma et al., 2022; Bolade et al., 2020). This reactivity of iron with phenolics is responsible for a change in organoleptic properties of the food and compromises iron bioavailability (Bovell-Benjamin & Guinard, 2003; McGee & Diosady, 2018a).

Several physical and chemical approaches are currently being used to control the reactivity of iron ions by limiting their exposure to reactive phenolics (Habeych et al., 2016). One strategy is the micro-encapsulation of soluble iron-containing salts (Zimmermann, 2004). However, encapsulated iron can lead to undesirable higher prices and therefore less acceptance by customers (Zuidam, 2012). Another approach for fortification of food products with iron is the use of strong molecular complexes such as FeEDTA (Ferrazone®) which reduces the reactivity of Fe ions while providing similar relative bioavailability as ferrous sulfate (Bothwell & MacPhail, 2004). However, the relatively high costs and the concern that EDTA compounds may negatively influence the metabolism of other essential minerals, or increase absorption of potentially-toxic minerals limit consumer acceptance (Allen et al., 2006). Another commonly used strategy is the use of water-insoluble, or poorly soluble salts such as iron (III) pyrophosphate (FePP) (McGee & Diosady, 2018b; Tian et al., 2016; van Leeuwen et al., 2012). In food research, FePP receives extensive attention and it is often

* Corresponding author.
E-mail addresses: n.moslehi@uu.nl (N. Moslehi), judith.bijlsma@wur.nl (J. Bijlsma), wouter.debruijn@wur.nl (W.J.C. de Bruijn), krassimir.velikov@unilever.com (K.P. Velikov), jean-paul.vincken@wur.nl (J.-P. Vincken), W.K.Kegel@uu.nl (W.K. Kegel).
[1] Equal contribution of the authors.

https://doi.org/10.1016/j.jff.2022.105066
Received 26 November 2021; Received in revised form 1 April 2022; Accepted 2 April 2022
Available online 8 April 2022

used in iron fortification of food products such as infant cereal and chocolate drink powders (Baars et al., 2015; Salgueiro & Boccio, 2013; Srinivasu et al., 2015). The low solubility of iron from FePP reduces the impact of FePP on the organoleptic properties of the fortified food but also results in low iron bioavailability (Moretti et al., 2006). Micronization (i.e., downsizing the particle size to micron range, e.g. 0.3–0.5 μm) and emulsification techniques have been used to improve the bioavailability of FePP. While the process of micronization has the advantage that it does not affect the organoleptic properties of the food, its high costs currently limit its use (Moretti et al., 2006; Shubham et al., 2020). Even though solubility of (micronized) FePP is limited in the pH range of 3–6, the addition of FePP to phenolic-rich foods or model systems still results in discoloration (Bijlsma et al., 2020; Habeych et al., 2016). FePP has also been incorporated with secondary minerals for higher efficiency and multipurpose applications (van Leeuwen et al., 2014; Zimmermann & Hilty, 2011). An example of this is the co-fortification of FePP with zinc sulfate in extruded rice (Hackl et al., 2017). Furthermore, FePP has been used in combination with citric acid or trisodium citrate in rice grains (Gupta et al., 2018) and with sodium pyrophosphate in bouillon cubes (Cercamondi et al., 2016) for relatively higher storage stability.

Inspired by nature, the main goal of this work is to integrate iron ions in an inorganic poorly water-soluble matrix of another mineral as a carrier. For example, anastasenkoite ($CaFe^{II}P_2O_7$) (Miyawaki et al., 2020) and anapaite ($Ca_2Fe^{II}(PO_4)_2{\cdot}4H_2O$) (Catti et al., 1979; Lafuente et al., 2014) are naturally occurring but not necessarily edible mixed phosphates of multivalent metal salts (Lafuente et al., 2014; Ravet et al., 2001). We particularly focus on pyrophosphate salts because pyrophosphate anions form colorless and/or white and water-insoluble compounds with most metals (Rossi et al., 2014; Tian et al., 2016; van Leeuwen et al., 2012). To maintain the organoleptic properties and (chemical) stability of the iron-fortified food, iron dissolution from the iron-containing compound should ideally be limited in the pH range from 3 to 7, which is the pH range of most common food and beverages (Habeych et al., 2016). The insolubility of the iron ions in the pH range from 3 to 7 will suppress iron-mediated reactivity in the food (Bijlsma et al., 2020). Additionally, to ensure bio-accessibility of iron, dissolution of iron from the iron-containing compound should be fast in gastric (i.e., pH 1–3) and/or intestinal (i.e., pH 6–8) conditions (Hurrell et al., 2002; Rohner et al., 2007; Wienk et al., 1999). It should be noted that although bio-accessibility (i.e., the quantity of iron in solution and available for absorption in the gastrointestinal tract) is a prerequisite for bioavailability, it cannot directly be correlated to iron bioavailability, which also includes digestion, absorption, and metabolism (Wienk et al., 1999). FePP salt has low solubility (<5%) at pH 3 with increased solubility to >99% at pH 7–8 (Tian et al., 2016) whereas the pyrophosphate salts of divalent metals, such as calcium pyrophosphate (CaPP), dissolve well (>99%) at pH 3 but are poorly soluble (<5%) at pH 7–8 (van Leeuwen, 2013). Doping of iron (III) oxide with calcium has previously shown improved iron solubility in dilute acid and sensory characteristics in fortified foods (Hilty et al., 2011; Zimmermann & Hilty, 2011). Additionally, van Leeuwen and co-authors have shown that incorporation of an excess of Mg in FePP (i.e., Mg:Fe(III) ratio 50:1), reduced its reactivity towards phenolics (van Leeuwen et al., 2014). Due to the reversed solubility character of CaPP and FePP salts, it is expected that the combination of Ca and Fe(III) in one matrix will result in unique pH-dependent dissolution behavior. Although any non-iron divalent metal (e.g. Zn, Ca, Mg, or Mn) could be used, Ca is selected due to its higher recommended nutrient intake and consequently less risk of overdosing compared to the other divalent metals (Allen et al., 2006; Joint FAO/WHO Expert Consultation: Vitamin and Mineral Requirements in Human Nutrition, 2004). Besides decreasing the reactivity of iron by embedding it in another less chemically reactive mineral carrier, the main advantage of these systems is that they can be used for simultaneous delivery of another essential mineral along with iron, in this case calcium.

In this study, we explore the possibility to design mixed Ca-Fe(III) pyrophosphate salts with the general formula, $Ca_{2(1-x)}Fe_{4x}(P_2O_7)_{(1+2x)}$ ($0 \leq x \leq 1$), as a potential delivery system for two essential minerals. To this end, we develop a detailed synthesis for and perform in-depth characterization of such mixed salts. The range of the ratios of iron to calcium is guided by the Recommended Dietary Allowance (RDA). Co-precipitation is used as a synthesis method in order to embed iron (III) ions homogenously into the calcium pyrophosphate matrix structure. After characterization of the salts, the pH dependence of the dissolution behavior of the mixed Ca-Fe(III) pyrophosphate salts with various Ca:Fe (III) ratios are investigated. Then, the effect of three food-relevant temperatures (23, 37, and 90 °C), as well as the dissolution time, are investigated. Finally, the designed salts are tested for their reactivity using a black tea model solution.

The main aim of this study is to design mixed Ca-Fe(III) pyrophosphate salts with three main properties: (i) maximum iron content in which no physical segregation occurs, (ii) increased solubility at gastric/intestinal pH, and (iii) reduced iron solubility at food pH and thus decreased reactivity compared to iron (III) pyrophosphate.

2. Materials and methods

2.1. Materials

Iron (III) chloride hexahydrate ($FeCl_3{\cdot}6H_2O$, >99 wt%), tetrasodium pyrophosphate decahydrate ($Na_4P_2O_7{\cdot}10H_2O$, >99 wt%), calcium dichloride ($CaCl_2$, >93 wt%), nitric acid (HNO_3, 65 wt%), 3-(2-pyridyl)-5,6-diphenyl-1,2,4-triazine-*p*,*p*′-disulfonic acid monosodium salt hydrate (i.e., ferrozine; ≥97 wt%), hydrochloric acid (HCl, 37 wt%), sodium hydroxide (NaOH, ≥98 wt%), and iron (II) sulfate heptahydrate ($FeSO_4{\cdot}7H_2O$, ≥99 wt%) were obtained from Sigma Aldrich (St. Louis, MO, USA). Ethanol absolute (≥99 wt%) and ascorbic acid (≥99 wt%) were obtained from VWR International (Radnor, PA, USA). The Milli-Q (MQ) water used was deionized by a Millipore Synergy water purification system (Merck Millipore, Billerica, MA, USA). The tea used for preparing the tea solutions was an Original English tea blend from Pickwick® (Amsterdam, The Netherlands).

2.2. Preparation of pure and mixed metal salts

2.2.1. Pure salts

Pure salts were synthesized as references for comparative purposes. The preparation procedure was a co-precipitation method similar to the methods described elsewhere (Rossi et al., 2014; van Leeuwen et al., 2012). Firstly, solutions of 0.857 mmol $FeCl_3{\cdot}6H_2O$ and 1.286 mmol $CaCl_2$ in 50 ml of MQ water were prepared independently. Following this, the solutions were added quickly (within 5 s) to a solution of 0.643 mmol $Na_4P_2O_7{\cdot}10H_2O$ (NaPP) in 100 ml of MQ water in order to prepare iron (III) pyrophosphate ($Fe_4(P_2O_7)_3$, FePP) and calcium pyrophosphate ($Ca_2P_2O_7$, CaPP), respectively. This was done while the NaPP solution was stirring vigorously (~400 rpm) with a magnetic stir bar. In both cases, a turbid white dispersion was formed a few seconds after the addition. The samples were then centrifuged at 3273*g* for 15 min in 50 ml volume polypropylene conical centrifuge tubes using an Allegra X-12R Centrifuge (Beckman Coulter, Brea, CA, USA). This was followed by washing the precipitate with MQ water twice. The sediment was then post-treated by ultrasonication at 40 kHz for 10 min using a CPX8800H ultrasonic cleaning bath (Branson Ultrasonics™, Brookfield, CT, USA), after which they were dried overnight in an oven at 45 °C (FePP: 59% yield, CaPP: 74% yield).

2.2.2. Mixed metal salts

The mixed Ca-Fe(III) salts were prepared by the same procedure as the pure salts, by addition of 50 ml of a mixed solution of $FeCl_3{\cdot}6H_2O$ and $CaCl_2$ in MQ water to a solution of NaPP with a fixed concentration of pyrophosphate ions (6.43 mM, 100 ml). Eight different salts

containing different Ca to Fe(III) ratios were prepared, generally coded as $Ca_{2(1-x)}Fe_{4x}(P_2O_7)_{(1+2x)}$ ($0 < x < 1$), for different theoretical x-values (i.e., 0.005, 0.006, 0.007, 0.011, 0.021, 0.051, 0.100 and 0.260, coded as Mix1 to Mix8). After adding the mixed solution to NaPP the eight solutions were stirred vigorously (~400 rpm) with a magnetic stir bar (final concentration of NaPP: 4.29 mM). In all ratios, a turbid white or off-white dispersion was formed a few seconds after the addition. The samples were then centrifuged, washed, post-treated in an ultrasonic bath, and dried in an oven following the same procedures as explained for the pure salts, see Section 2.2.1. It is worth recalling here that the x-values in the general formula indicate the mineral composition of the salts. These values were chosen based on average nutritional requirements for the human body (i.e., 1000 mg calcium and 15 mg iron intake per day (Ross et al., 2011). Consequently, the mole ratios were calculated based on which the x-value was found in the structural formula. The molar ratio of total metal ions (i.e., [Ca] + [Fe], final concentration: 8.573 mM) to pyrophosphate ions was based on the stoichiometry of CaPP. The average yield of the prepared mixed salts was 67.3 ± 4.2%. Standard deviation was calculated based on three independent syntheses of all the mixed salts.

2.3. Characterization methods

2.3.1. Transmission electron microscopy (TEM) and energy-dispersive X-ray spectroscopy (EDX)

Water dispersions of the salts were dried on a carbon-coated copper grid and analyzed by transmission electron microscopy (TEM) and energy-dispersive X-ray spectroscopy (EDX). This was performed on a Talos™ F200X (Thermo Fisher Scientific, San Jose, CA, USA) operated at 200 kV. The elemental composition of the mixed salts was obtained from EDX and used for finding the experimental x-value based on the general formula of the mixed salts. The ratios of the atomic percentages (i.e., Ca/Fe = 2(1-x)/4x, Ca/P = 2(1-x)/2(1+2x), Fe/P = 4x/2(1+2x)) were used to find x in the structural formula $Ca_{2(1-x)}Fe_{4x}(P_2O_7)_{(1+2x)}$. The average x-value for each mixed salt was reported with a standard deviation based on 3 replicate preparations of the salts and 3 independent measurements. The average x-values were incorporated in the general formula of the mixed Ca-Fe(III) pyrophosphate salts to obtain the final chemical formula of the salts. For the salts with heterogeneous morphology, this procedure was done separately on the different morphological phases.

2.3.2. High-angle annular dark field scanning TEM (HAADF-STEM)

High-angle annular dark-field scanning TEM (HAADF-STEM) was performed on a Talos™ F200X (Thermo Fisher Scientific, San Jose, CA, USA) operated at 200 kV. The elemental mapping was recorded by use of assigning a color to each element. Color indications are as follows: calcium: green, iron: red, and phosphorus: blue.

2.3.3. X-ray diffraction (XRD) spectroscopy

The dried powders of the salts were analyzed at room temperature with an AXS D2 Phaser powder X-ray diffractometer (Bruker®, Billerica, MA, USA), which was equipped with a LYNXEYE® detector in Bragg-Brentano mode. The radiation used was cobalt $K\alpha_{1,2}$, $\lambda = 1.79026$ Å, operated at 30 kV, 10 mA for $2\theta = 5$ to 70°. A silicon holder was used and the measurements were repeated twice on the salts from independent synthesis batches.

2.3.4. Fourier transform infrared (FT-IR) spectroscopy

FT-IR measurements were done on dried powders of the samples by an FT-IR spectrometer (PerkinElmer, Waltham, MA, USA), using the KBr pellet technique (Drenchev et al., 2020). 2.5 mg of each salt was mixed thoroughly with 250 mg of KBr (FT-IR grade) and dried in an oven at 60 °C overnight. Pellets were prepared using a press and the measurements were done in independent duplicate. The interferograms were accumulated over the spectral range of 1600 – 400 cm^{-1} using a nominal resolution of 4 cm^{-1}, with a background spectrum recorded before each measurement.

2.4. Dissolution behavior of iron in FePP and the mixed Ca-Fe(III) pyrophosphate salts

To perform the iron dissolution measurements, the synthesis of the pure FePP and CaPP as well as the mixed Ca-Fe(III) pyrophosphate salts with measured $0.14 \leq x \leq 0.35$ were up-scaled, **Method S1** of **Supplementary material**. The dried powders of the salts were then redispersed by stirring (~250 rpm) with a magnetic stir bar in MQ water (final concentrations: 10 mg/ml). Next, the pH of the dispersions was adjusted using a pH-stat device (Metrohm, Herisau, Switzerland) by the addition of 0.1 M HCl or 0.1 M NaOH. Subsequently, all dispersions were incubated at 1000 rpm using an Eppendorf Thermomixer® F1.5 (Eppendorf, Hamburg, Germany) at pH values ranging from one to eleven (steps of one pH unit), over time (1, 2, and 48 h), and at three different temperatures (23, 37, and 90 °C). After incubation, the pH of each sample was measured again to determine the final pH. Finally, the samples were centrifuged at 15000*g* for 10 min using an Eppendorf Centrifuge 5415R and the supernatants were separated to quantify the dissolved iron concentration.

2.4.1. Iron concentration measurement by ferrozine-based colorimetric assay

Total iron in solution was quantified using a ferrozine-based colorimetric assay (Stookey, 1970). Binding of Fe(II) to 3-(2-pyridyl)-5,6-diphenyl-1,2,4-triazine-*p*,*p*′-disulfonic acid (i.e., ferrozine) results in the formation of a complex with absorbance at 565 nm (Bijlsma et al., 2022). To ensure the reduction of Fe(III) to Fe(II), first an excess of ascorbic acid (50 μL, 100 mM) was added to 50 μL sample (supernatant). After 30 min incubation of the sample with ascorbic acid, ferrozine (50 μL, 10 mM) was added. Samples were transferred to 96-well microplates and the absorbance at 565 nm was measured at room temperature in a SpectraMax M2e (Molecular Devices, Sunnyvale, CA, USA). All measurements were performed in duplicate and quantification of total dissolved iron was performed based on intensity ($A_{565\ nm}$) with a calibration curve of $FeSO_4$ (0.0078–1 mM, $R^2 > 0.99$). It was confirmed that the presence of the Ca ion did not interfere with the quantification of total iron (**Fig. S1** of **Supplementary material**). The pH of the samples was measured after the addition of ascorbic acid and ferrozine. Most samples had a pH of 2.7, except for the samples that were prepared at very acidic conditions (i.e., pH < 2). The pH of these samples after the addition of ascorbic acid and ferrozine was 1.7 ± 0.3. At this pH, less Fe (II)-ferrozine complex is formed (Stookey, 1970). We corrected the absorbances of these acidic samples using the pH-dependent absorbance factors previously reported for the Fe(II)-ferrozine complex formation (Stookey, 1970). The iron quantification by the ferrozine assay was verified independently using inductively coupled plasma–atomic emission spectroscopy (ICP-AES), **Method S2** of **Supplementary material**.

To test if the trend in iron dissolution was statistically significant, ANOVA analysis was performed using IBM SPSS Statistic v23 software (SPSS Inc., Chicago, IL, USA). Tukey's *post hoc* comparisons (significant at $p < 0.05$) were carried out to evaluate the significance of differences in iron concentration.

2.5. Assessment of the reactivity of selected mixed salts in a black tea solution

To assess the reactivity of the iron in the mixed Ca-Fe(III) pyrophosphate salts, a black tea solution was used as a model system. Ground tea leaves of Original English blend (Pickwick®) were added to boiling MQ water (1 g of tea leaves in 100 ml of water). After stirring for 3 min, the tea leaves were filtered out using 1541–125 cellulose filter papers (Whatman®, Maidstone, UK). Selected mixed and pure FePP salts with a normalized concentration of iron (i.e., 1.05 mg Fe in 100 ml tea) were

added to the tea solution (pH 5.13 ± 0.13). For comparison, CaPP with a normalized concentration of 2.31 mg Ca in 100 ml tea (i.e., the concentration of Ca in the salt with the highest calcium content) was added as well. After stirring for 10 min using an RCT basic stirrer (IKA-Werke, Staufen, Germany), the tea solutions were filtered first over Whatman® cellulose filter papers and second over a 17845-ACK Minisart® NY polyamide (nylon) filter with 0.2 μm pore size, (Sartorius, Göttingen, Germany). During the procedure, the temperature was kept constant at approximately 90 °C in all steps. The residues on the filter papers were washed with ethanol to remove any unbound phenolics from the particle surface. The discoloration of the filtered tea solutions was quantified by ultraviolet–visible light (UV–Vis) spectroscopy at room temperature. UV–Vis spectra of the tea solutions were recorded on a Lambda-35 spectrophotometer (PerkinElmer, Waltham, MA, USA), using quartz cuvettes. The increase in absorbance at 550 nm compared to the blank black tea solution was used to quantify the iron-phenolic complexation (McGee & Diosady, 2018b). All the measurements were done in independent triplicates and the average values along with standard deviations were reported. The colors of the tea solutions were visualized by taking an image of all tea solutions standing next to each other illuminated with a uniform light source at room temperature. The images were evaluated using an online color conversion tool (https://imagecolorpicker.com/) and converted to the $L^*a^*b^*$ color space (i.e., L^* dark or light, a^* red vs. green, b^* yellow vs. blue) (**Table S1** of **Supplementary material**).

The concentration of the iron released from the salts in the tea solutions was measured by elemental analysis using ICP-AES. ICP-AES was performed on the tea solutions using an Optima 8300 instrument (PerkinElmer, Waltham, MA, USA). Electrodeposited samples were dissolved in 10 ml of a 2% HNO_3 solution to achieve optimal measurement concentration ranges. The measurements were performed in triplicate. Statistical analysis was carried out to evaluate the significance of differences in iron concentration (significant at $p < 0.05$).

3. Results and discussion

3.1. Characterization of the pure calcium and iron (III) pyrophosphate salts

The morphology of the pure CaPP and FePP salts was analyzed by electron microscopy (Fig. 1). The dried dispersions of CaPP and FePP showed noticeably different morphologies. The TEM images for CaPP showed large micron-sized needle-shaped aggregates (Fig. 1**a**), which is in line with a previous study (Gras et al., 2013). However, the TEM image results for FePP showed formation of large interconnected aggregates of roughly 25 nm irregularly shaped particles, see Fig. 1**b**.

It has been previously shown that the degree of crystallinity in metal pyrophosphate particles can strongly depend on the valence of the metal ion (van Leeuwen et al., 2012). This has been confirmed by XRD and FT-IR spectra of the pure CaPP and FePP salts in this work as well. The X-ray diffraction pattern for CaPP indicated clear signals of crystallinity, while the spectrum for FePP showed only noise and a broad peak indicating an amorphous structure for this salt (Fig. 1**c**). The XRD spectra of CaPP and FePP are consistent with previous studies (Rossi et al., 2014; van

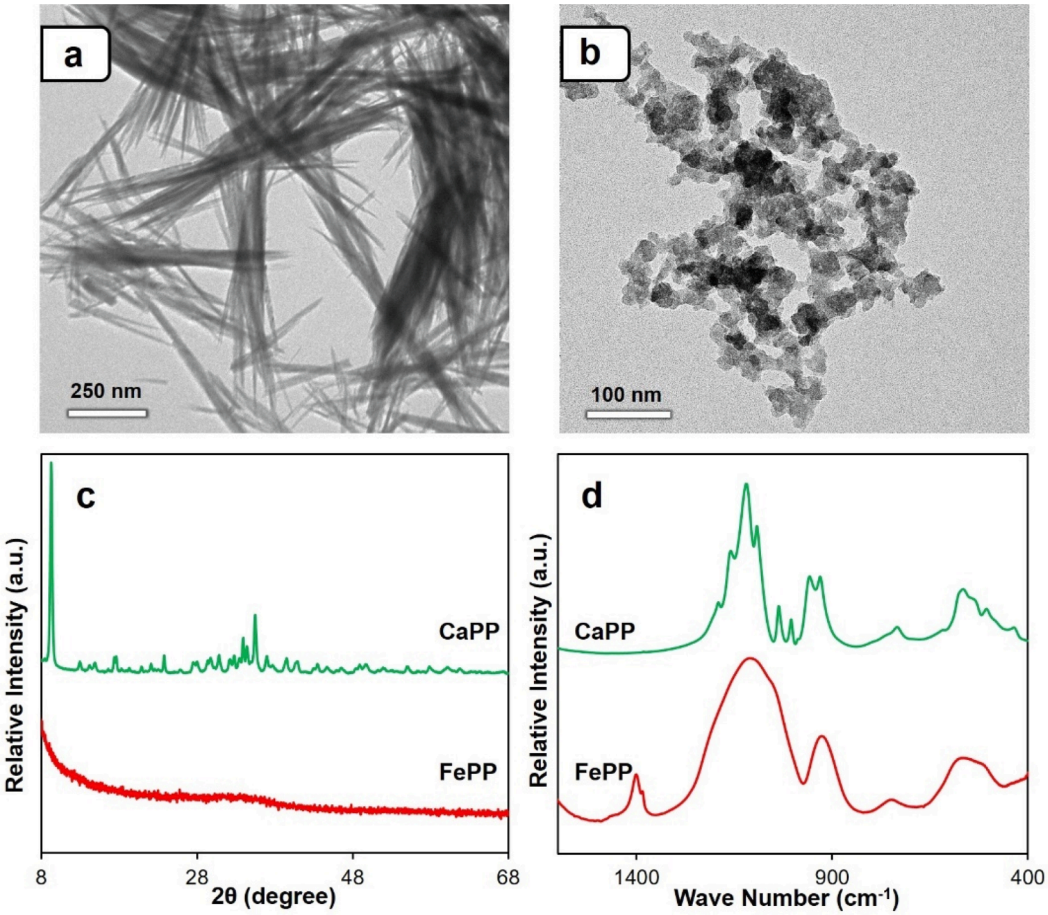

Fig. 1. TEM images of (a) CaPP and (b) FePP, representing the difference between calcium and iron (III) pyrophosphate salts morphologies. CaPP forms large aggregates of micron-sized needles whereas FePP yields large interconnected aggregates of approximately 25 nm irregularly shaped particles. (c) Comparison between XRD spectra of the two pure pyrophosphate salts shows that CaPP is crystalline, whereas FePP is amorphous. (d) For the same reason, the FT-IR absorbance of the chemical bonds in the pyrophosphate ions appear sharp and strong for CaPP, and broad and smooth for FePP.

Leeuwen et al., 2012). However, we observed a strong, sharp signal at approximately $2\theta = 9.2^{\circ}$ for CaPP (Fig. 1**c**) that was not observed previously (Rossi et al., 2014; van Leeuwen et al., 2012). This could be because of different crystalline structures from the fast co-precipitation method compared to the preparation of colloidal particles (van Leeuwen et al., 2012) or solid-state preparation at high temperatures (El Kady et al., 2009). Moreover, ultrasonication treatment on the salts could have led to induced crystallinity and heterogenous nucleation (Luque de Castro & Priego-Capote, 2007). The observed amorphous structure of FePP is suggested to be a result of the so-called valence mismatch of the metal (Fe^{3+}) and pyrophosphate ($P_2O_7^{4-}$) ions (Rossi et al., 2014). Therefore, the complicated stoichiometry to reach neutrality results in an amorphous matrix for FePP in a fast co-precipitation process, while calcium and pyrophosphate ions can form electroneutral crystalline unit cells more easily (van Leeuwen et al., 2012).

The details of chemical bonding in both the CaPP and FePP were investigated by FT-IR spectrometry (Fig. 1**d**). The FT-IR spectrum for CaPP showed sharp and well-defined bands, whereas the peaks appeared broad and smooth for FePP at the same wavenumbers. The sharper and well-defined bands were expected for crystalline materials. Spectral broadening in FePP was a result of the pyrophosphates having to accommodate more types of bonding to reach neutrality (Lai et al., 2011), and indicates the amorphous nature of FePP (Singh et al., 2017; van Leeuwen et al., 2012). Despite different broadness, peak positions of the main peaks matched with each other because the pyrophosphate groups are the main vibrationally active species. The characteristic peaks attributed to bending for O-P-O bonds in the P_2O_7 groups appeared around 500–600 cm^{-1}. The signals observed at 745 and 945 cm^{-1} were assigned to symmetric and asymmetric vibrations in P-O-P, respectively, and the peaks in the range of 1000 to 1200 cm^{-1} corresponded to P-O stretching vibration frequencies. All the peaks observed for the $P_2O_7^{4-}$ anion are similar to previous reports (Kosova et al., 2017; Singh et al., 2017; Zheng et al., 2014).

3.2. Characterization of the mixed Ca-Fe(III) pyrophosphate salts

The morphology and chemical composition of the mixed metal salts, designed with $0.005 \leq x \leq 0.260$ in the general formula $Ca_{2(1-x)}Fe_{4x}(P_2O_7)_{(1+2x)}$, (coded as Mix1-Mix8) were characterized by electron microscopy (Fig. 2**)**. TEM images of the salt with the lowest iron content, Mix1, indicated a single phase of micron-sized needle-shaped aggregates (Fig. 2**a**). The measured x-value was 0.009, as determined from EDX measurements (Fig. 2**b**).

Detailed analysis of the TEM images and EDX results suggest that integrating Fe(III) as a second metal in the CaPP matrix can yield local segregation and coexistence of two morphological phases: a crystalline needle-shaped phase with relatively low Fe content, and amorphous irregularly shaped aggregates with higher Fe content (i.e., higher x-value). Samples Mix2 to Mix5 appeared to be a mixture of an iron-rich phase (mostly irregularly shaped particles) and a calcium-rich phase (needle-shaped particles) (Fig. 2**a**). EDX quantification indicated that the sample Mix2 is a mixture of micron-sized needles with $x = 0.012$ and irregularly shaped aggregates with $x = 0.455$ (Fig. 2**b**). Similarly, in both samples, Mix3 and Mix4, micron-sized needles and irregularly shaped aggregates were in coexistence, and the latter yielded higher x-values. In the case of the sample Mix5, the measured x-value was equal to 0.020 for the irregularly shaped aggregates, while the ellipse-shaped aggregates remained ill-defined in this salt. These ill-defined particles

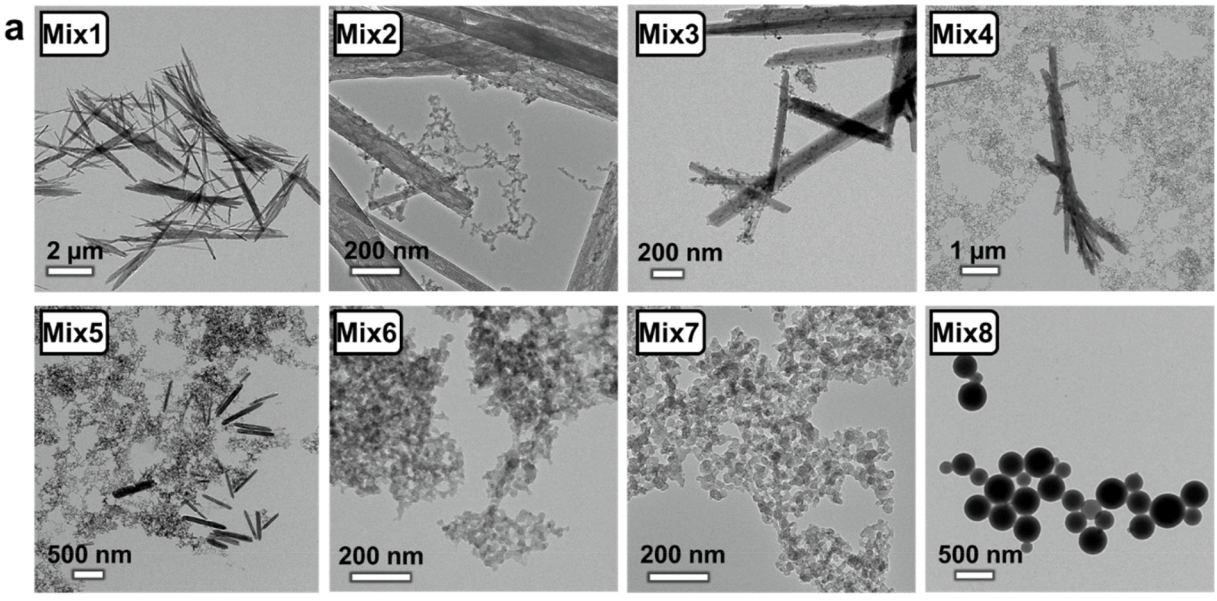

b

Salt code	Mix1	Mix2	Mix3	Mix4	Mix5	Mix6	Mix7	Mix8
Designed x	0.005	0.006	0.007	0.011	0.021	0.051	0.10	0.26
Measured x	0.009±0.001 (N)	0.012±0.004 (N) 0.455±0.007 (I)	0.017±0.007 (N) 0.223±0.089 (I)	0.003±0.001 (N) 0.033±0.001 (I)	ill-defined (E) 0.020±0.005 (I)	0.140±0.040(I)	0.150±0.050 (I)	0.350±0.070 (S)

Fig. 2. (a) Morphology of the mixed Ca-Fe(III) pyrophosphate salts with the general formula $Ca_{2(1-x)}Fe_{4x}(P_2O_7)_{(1+2x)}$, coded as Mix1 to Mix8, obtained from TEM imaging. Comparison indicates that the iron-containing salts Mix1 and Mix6 to Mix8 are present in identical homogenous morphologies, whereas the samples Mix2 to Mix5 show segregation into two coexisting structural phases. (b) The measured x-value for the mixed Ca-Fe(III) pyrophosphate salts obtained from EDX quantification. Salts Mix2 to Mix5 show different measured x-values for the coexisting morphologies, while the salts Mix1 and Mix6 to Mix8 have identical x-values. The morphology of the aggregates is indicated by (N) needle-shaped, (I) irregularly shaped, (E) ellipse-shaped, and (S) spherical.

can be oxide or hydroxide sediments of iron (III) formed during the synthesis or drying procedures (Fig. 2**a** and **Fig. S2** of **Supplementary material**). The formation of the Ca-rich and Fe-rich phases of particles, resulting in different measured x-values (from EDX quantification), might be explained by the possibility for phase separation in the resulting solid solutions (Li, 2018; Tan et al., 2009).

The salts Mix6 to Mix8 showed uniform morphologies and chemical compositions. For Mix6 and Mix7, irregularly shaped aggregates of 50 to 80 nm in size were observed, (Fig. 2**a**). These morphologies were similar to the FePP particles morphology and the x-values corresponding to these two salts were measured to be 0.140 and 0.150, respectively (Fig. 2**b**). Interestingly, TEM images of the mixed salt with the highest iron content, Mix8, showed almost perfect spherical particles (Fig. 2**a**), for which the x-value was measured to be 0.350 from EDX quantification (Fig. 2**b**). The formation of well-defined needle-shaped or spherical particles can be caused by the ultrasonication treatment in the preparation method. Ultrasound energy fields have been shown to aid shape changes in particles by locally overcoming energy barriers for specific structures (Suslick et al., 1996) (**Fig. S3** of **Supplementary material**). The possible effects of ultrasonication is currently being studied separately.

The elemental distribution in the mixed Ca-Fe(III) pyrophosphate salts with uniform morphologies (i.e., measured $0.14 \leq x \leq 0.35$) was explored by HAADF-STEM. Homogenous distribution of the elements Ca, Fe, and P was observed by elemental mapping of the mixed salts Mix6 to Mix8 (Fig. 3**a**). The corresponding dark-field scanning TEM images of each elemental mapping are shown in Fig. 3**b** as well.

The crystallinity of the mixed Ca-Fe(III) pyrophosphate salts was investigated by X-ray powder diffraction analysis (Fig. 4**a**). The XRD spectra of the mixed salts were not in agreement with any existing XRD reference patterns in the international center for diffraction data (ICDD, https://www.icdd.com). In general, comparing the XRD patterns of the mixed salts to the diffraction peaks of the CaPP specified the gradual transformation of crystalline structures upon increasing iron content in these samples. Similar to the CaPP, the XRD patterns of the mixed Ca-Fe (III) pyrophosphate salts Mix1 to Mix5 (i.e., measured $0 \leq x < 0.14$), show consistent sharp signals which were clear signs of crystalline structures in these salts (van Leeuwen et al., 2012). The intensity of the diffraction peak at 9.2° (peak a), which appeared sharp and strong for CaPP, decreased in the mixed Ca-Fe(III) pyrophosphate salts. Ultimately, this peak dissapeared in the salt Mix4.

The diffraction patterns of the mixed salts in the range of 13–15° (peaks b-d), 22.5° (peak e), and 32–34° (peaks f-h) indicate the presence of distinct crystalline phases and polymorphs in their structures. Peaks b, d, and g appeared with maximum intensity in the salt Mix1. A gradual decrease was observed upon increasing iron content in the salts Mix2, Mix3, and Mix4, and eventually the peaks disappeared in the salt Mix5. Furthermore, the reflections c, e, f, and h slightly grew and reached a maximum at Mix4. However, the intensity of these peaks was drastically reduced in the salt Mix5 and reached zero in the samples Mix6-Mix8 ($0.14 \leq x \leq 0.35$).

Finally, the mixed Ca-Fe(III) pyrophosphate salts Mix6 to Mix8 ($0.14 \leq x \leq 0.35$) and FePP ($x = 1$) showed no distinct diffraction peaks in their X-ray diffraction spectra which was a clear indication of amorphous structure in these salts. The one exception to this was in the sample Mix7 ($x = 0.15$) which showed two weak absorbance peaks at 10 and 14°. This could be related to the ultrasonication-induced crystallization of the pyrophosphate salts resulting from the preparation method in this work (Luque de Castro & Priego-Capote, 2007; van Leeuwen et al., 2012) which is out of the scope of the present work. Nonetheless, no sign of crystalline needle-shaped aggregates with iron or calcium dominant regions was observed in the TEM images of this sample (Fig. 2**a**).

The details of chemical bonds in the structure of the mixed Ca-Fe(III) pyrophosphate salts were explored by FT-IR spectroscopy (Fig. 4**b**). The analysis of the FT-IR spectra of the mixed salts showed that peak

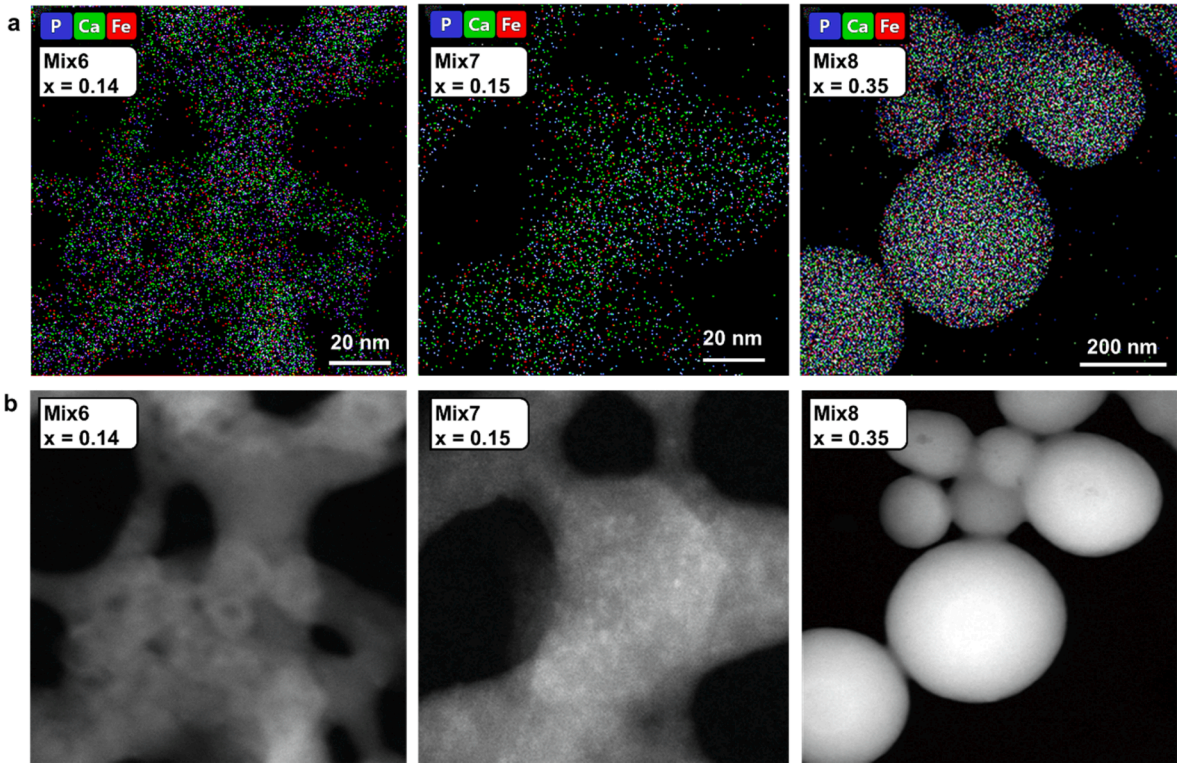

Fig. 3. (a) Elemental mapping performed by HAADF-STEM on Mix6 ($x = 0.14$), Mix7 ($x = 0\ 0.15$) and Mix8 ($x = 0.35$). Color indications are as follows: calcium (Ca): green; iron (Fe): red; and phosphorous (P): blue. Elemental mapping clearly shows homogeneous distribution of the elements in these salts. (b) The corresponding dark-field images. (For interpretation of the references to color in this figure legend, the reader is referred to the web version of this article.)

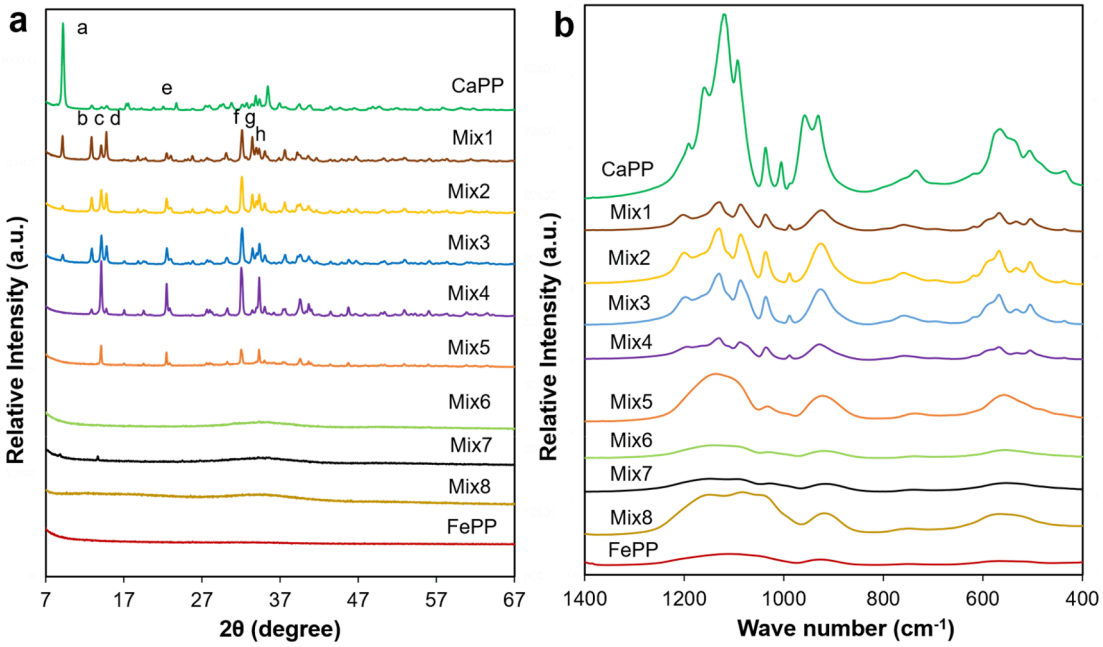

Fig. 4. (a) XRD and (b) FT-IR spectra of the mixed Ca-Fe(III) pyrophosphate salts with the general formula $Ca_{2(1-x)}Fe_{4x}(P_2O_7)_{(1+2x)}$ ($0 < x < 1$). The spectra of the pure CaPP ($x = 0$) and FePP ($x = 1$) are shown for comparison. (a) For the salts Mix1-Mix5 and CaPP ($0 \leq x < 0.14$) samples show clear signals for crystalline structure. The spectra for the salts Mix6-Mix8 and FePP ($0.14 \leq x \leq 1$) exhibit broad smooth peaks which indicate amorphous structures. (b) Positions of the peaks correspond to the chemical bonds in the pyrophosphate ions coincide between the mixed salts. Sharp and strong peaks are observed for the crystalline pyrophosphate salts Mix1-Mix5 and CaPP ($0 \leq x < 0.14$), whereas broad and smooth peaks are obtained for the amorphous salts Mix6-Mix8 and FePP ($0.14 \leq x \leq 1$).

positions coincided between the salts because the vibrations only correspond to the chemical bonds present in the pyrophosphate ions. Pyrophosphate vibrations showed sharp and strong peaks for the crystalline salts with measured $0 \leq x < 0.14$, while the same peaks appeared broad and smooth for amorphous samples with measured $0.14 \leq x \leq 1$. The peak positions coincided with the values observed for pyrophosphate in the individual CaPP and FePP salts as discussed in Section 3.1.

3.3. Dissolution behavior of iron in FePP and the mixed Ca-Fe(III) pyrophosphate salts

The challenge of novel iron-containing salts is to ensure appropriate pH-dependent dissolution behavior of the iron compound. To limit iron-mediated reactions, while ensuring bio-accessibility, the iron dissolution should be limited at food pH (3–7) and fast at gastric pH (1–3) and/or intestinal pH (6–8). Therefore, we investigated the pH-dependent dissolution behavior of FePP and mixed Ca-Fe(III) pyrophosphate salts. According to what was discussed above, the mixed Ca-Fe(III) pyrophosphate salts Mix6-Mix8 were most desirable for the main application of this study as they presented uniform morphologies and homogenous distribution of the elements (i.e., Ca, Fe, P). On the contrary, the samples Mix2-Mix5 with two coexisting phases were not further investigated for their solubility or reactivity. This is because of the presence of multiple structural phases and hence different chemical compositions that can result in unpredictable dissolution or reactivity behaviors of the salts. Furthermore, despite having a homogeneous morphology, sample Mix1 is not particularly suitable for food application because of the specific shape and size of its aggregate, beside having a very low iron content (Marian et al., 2021; van Leeuwen et al., 2012).

The three selected mixed Ca-Fe(III) pyrophosphate salts were prepared using the up-scaled synthesis method (**Method S1**, **Supplementary material**). Up-scaling the synthesis did not affect the morphology or the elemental homogeneity in the salts (results not shown). The dissolution behavior of FePP ($x = 1$) and the three mixed Ca-Fe(III) salts Mix6 to Mix8 ($x = 0.14$, 0.15, and 0.35), was evaluated as a function of pH by UV–Vis spectroscopy using the ferrozine assay (Stookey, 1970). Quantification of the accuracy of total iron determination by the ferrozine assay was verified by comparison with the ICP-AES method (**Fig. S4** of **Supplementary material**). The iron concentrations measured by both methods were found to be in good agreement ($R^2 = 0.99$). Due to the affordability, availability, and high throughput of the ferrozine assay it was decided to use the ferrozine assay for further experiments. The aqueous dissolution behavior of iron from FePP and the three mixed Ca-Fe(III) pyrophosphate salts was evaluated in the pH range from 1 to 10 (Fig. 5**a**).

In the pH range 2–5.5, soluble iron concentrations from FePP were below 0.50 mM (Fig. 5**a**). The limited solubility in this pH range is likely due to the presence of the solid species $Fe_4(P_2O_7)_3$ (Jiang et al., 1998; Tian et al., 2016). Below pH 2, iron dissolution from FePP increased to 1 mM due to the presence of ionic Fe(III) and the formation of soluble ferric pyrophosphate complexes (i.e., $FeH_3P_2O_7^{2+}$ and $FeH_2P_2O_7^{+}$) (Flynn, 2002; Jiang et al., 1998). Increased dissolution to 3.0 mM at pH > 5.5 could be explained by the formation of $Fe(HP_2O_7)_2^{3-}$, which is one of the soluble Fe(III)-pyrophosphate species (Jiang et al., 1998; Sun et al., 2020).

For Mix6 ($x = 0.14$) and Mix7 ($x = 0.15$) lower dissolved iron concentration (<0.25 mM) was observed at the food-relevant pH values (i.e., pH 3–7). This indicated that the ternary complex of $Ca_{2(1-x)}Fe_{4x}P_2O_{7(1+2x)}$ with $x = 0.14$ and 0.15 shows lower solubility at pH 3–7 compared to FePP. The lower amounts of dissolved iron at pH 3–7 for the mixed salts are desirable for application in food, as it could potentially lead to reduced iron-mediated reactivity of the food products upon iron fortification. For Mix8 ($x = 0.35$), similar or even higher dissolution of iron was observed in the food-relevant pH range compared to FePP. These results indicate that in the mixed Ca-Fe(III) pyrophosphate salts the x-value should be ≤ 0.15 to reduce iron dissolution at pH 3–7.

Interestingly, as the calcium content in the mixed salts increased, the salts showed enhanced iron solubility in the gastric pH range (1–3). For Mix6 ($x = 0.14$) and Mix7 ($x = 0.15$), an increase in dissolved iron of at least a fourfold compared to FePP was observed at pH 1. Higher quantities of total soluble iron at pH 1–3 and/or pH 6–9 are indicative of better bio-accessibility in the gastric and intestinal environment,

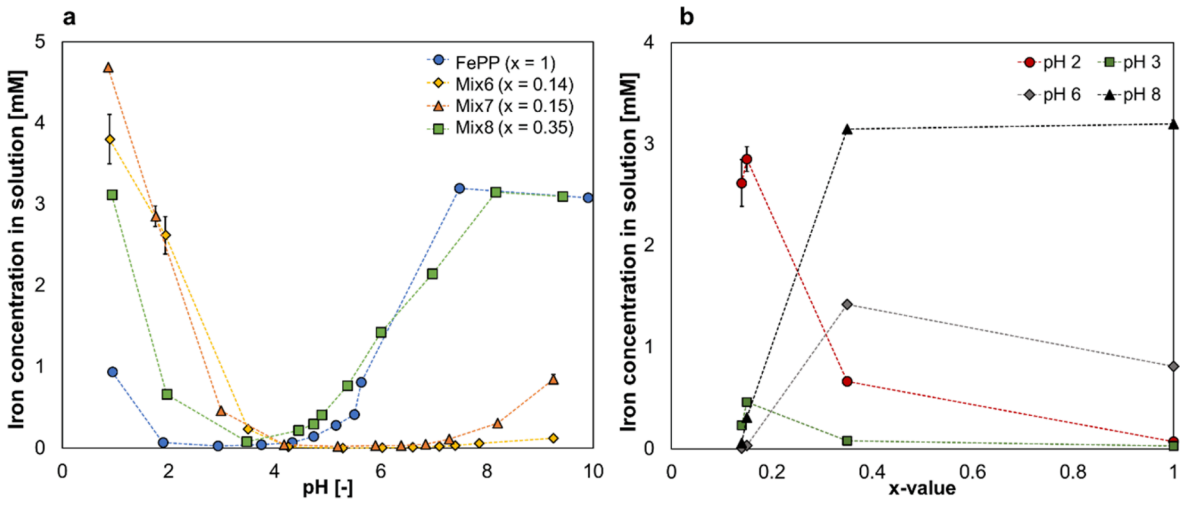

Fig. 5. (a) Dissolution of iron from FePP and mixed Ca-Fe(III) pyrophosphate salts Mix6 (x = 0.14), Mix7 (x = 0.15), and Mix8 (x = 0.18) as a function of pH. (b) Dissolution of iron from the salts as a function of x-value at pH 2, pH 3, pH 6, and pH 8. (a) Compared to FePP, Mix6 (x = 0.14) and Mix7 (x = 0.15) have a lower iron solubility at food-relevant pH (3–7), whereas at gastric pH (1–3), the salts show enhanced iron dissolution up to a fourfold increase. (b) Lower x-values (i.e., ≤ 0.15) have higher iron dissolution at low pH (i.e., 2 and 3). Howere, the salts with higher x-values (i.e., 0.35 and 1.0) yielded the highest iron concentrations in solution at high pH (i.e., 6 and 8).

respectively (Hurrell et al., 2002; Rohner et al., 2007; Swain et al., 2003; Tian et al., 2016; Wienk et al., 1999). At pH > 6, the opposite behavior was observed compared to acidic pH, with the highest iron dissolution for FePP and Mix8 (x = 0.35) salts, and lowest for Mix6 (x = 0.14). Even though the dissolution of iron from Mix6 (x = 0.14) and Mix7 (x = 0.15) was decreased compared to FePP at intestinal pH, the poor iron solubility of these salts at pH 3–7 and increased dissolution at pH 1–3 (Fig. 5**a**) indicates that these salts likely cause less organoleptic changes in food and are expected to show adequate bio-accessibility in the stomach (Hurrell et al., 2002; Swain et al., 2003). It has previously been shown that *in vitro* solubility of Fe-containing salts at pH 1 is a good indicator for *in vivo* Fe uptake by rats (Rohner et al., 2007).

Overall, these results indicate that increasing the proportion of calcium in the mixed pyrophosphate salts promotes the dissolution at low pH (1–3), whereas increasing the proportion of iron promotes dissolution at high pH (6–9). This is in line with previous results obtained for pure pyrophosphate salts, in which pure CaPP and FePP salts showed inverse pH-dependent solubility (van Leeuwen, 2013). The dissolution behavior of iron from FePP and mixed Ca-Fe(III) pyrophosphate salts was evaluated as a function of the x-value in $Ca_{2(1-x)}Fe_{4x}P_2O_{7(1+2x)}$. Fig. 5**b** shows the dissolution of iron from the salts as a function of x-value at four representative pH values (i.e., pH 2 for gastric conditions, pH 3 and 6 for food, and pH 8 for intestinal conditions). Lower x-values (i.e., ≤ 0.15) tend to have higher iron dissolution at low pH (i.e., 2 and 3). Furthermore, the salts with higher x-values (i.e., 0.35 and 1) yielded the highest iron concentrations in solution at high pH (i.e., 6 and 8). These findings show that the mixed Ca-Fe(III) pyrophosphate salts possess pH-dependent dissolution behavior which can be finetuned to the desired application by changing the x-value.

3.4. Effect of temperature and time on dissolution behavior of iron in the Ca-Fe(III) pyrophosphate salts

To effectively apply the Ca-Fe(III) pyrophosphate salts in fortified food products the pH-dependent dissolution at pH 3–7 must be limited during storage (23 °C), consumption (37 °C), and cooking (90 °C). Therefore, the effect of temperature on iron dissolution from FePP and the mixed Ca-Fe(III) pyrophosphate salts was investigated by incubating the samples at different temperatures (23, 37, and 90 °C) (Fig. 6**a**). Overall, no significant change ($p > 0.05$) in iron dissolution in the pH range 1–10 was observed upon elevating the temperature from 23 °C to 37 °C. This is in line with a previous study, that observed no change in the dissolution of Fe(III) from FePP upon elevating the temperature from 23 °C to 50 °C (Wilhelmy et al., 1985). Increasing the incubation temperature to 90 °C resulted in a significant ($p < 0.05$) increase in dissolved iron from FePP at pH 1 and 5.5 (Fig. 6**a**). The iron dissolution for Mix8 (x = 0.35) at pH ~ 7 also increased at 90 °C.

The iron dissolution of Mix6 (x = 0.14) and Mix7 (x = 0.15) decreased at pH 1–2 after heating at 90 °C. Possibly the ionic Fe(III) that is present in solutions of these mixed salts at pH < 3 underwent hydrolysis to insoluble species, which has been well-documented for Fe(III) at elevated temperatures (Dousma & De Bruyn, 1976; Flynn, 2002). For the mixed salts with x ≤ 0.15, iron concentration in solution remained similar at elevated temperatures at pH 3–7. Therefore, these mixed salts could potentially be used for cooking without an increase in reactivity.

Monitoring time-dependent iron concentration in the solutions pointed to no remarkable difference between iron dissolution for one and two hours of incubation (Fig. 6**b**). Over 48 h of incubation, dissolution remained constant at all pH ranges for all salts except for FePP with a significant ($p < 0.05$) increase at pH < 2 and pH 5–6 after 48 h.

3.5. Assessment of the reactivity of selected mixed salts by discoloration of a black tea solution

Black tea was chosen as a model system to investigate the reactivity of the mixed Ca-Fe(III) pyrophosphate salts in foods as, after water, it is the most widely consumed beverage in the world (Dueik et al., 2017). Black tea contains a considerable amount of phenolics that can trigger discoloration in the presence of iron ions, via iron-mediated complexation and oxidation (Bijlsma et al., 2022; McGee & Diosady, 2018a; Wang et al., 2015).

The black tea model solution was exposed to the three selected mixed Ca-Fe(III) pyrophosphate salts (i.e., Mix6, Mix7, and Mix8), as well as the pure CaPP and FePP salts (final pH of the solutions: 5.13 ± 0.13). Because the mixed salts Mix6 (x = 0.14) and Mix7 (x = 0.15) showed poor solubility at food-relevant pH, they were expected to show less reactivity and therefore less discoloration upon food fortification. The discoloration of the tea solution, caused by iron ions released from the salts after filtration is shown in Fig. 7**a**. Exposing the tea solutions to 1.05 mg Fe in the form of the pure FePP and mixed Ca-Fe(III) pyrophosphate salts for 10 min, resulted in the darkening of the tea solutions compared to the reference, the pure black tea solution. The visual color

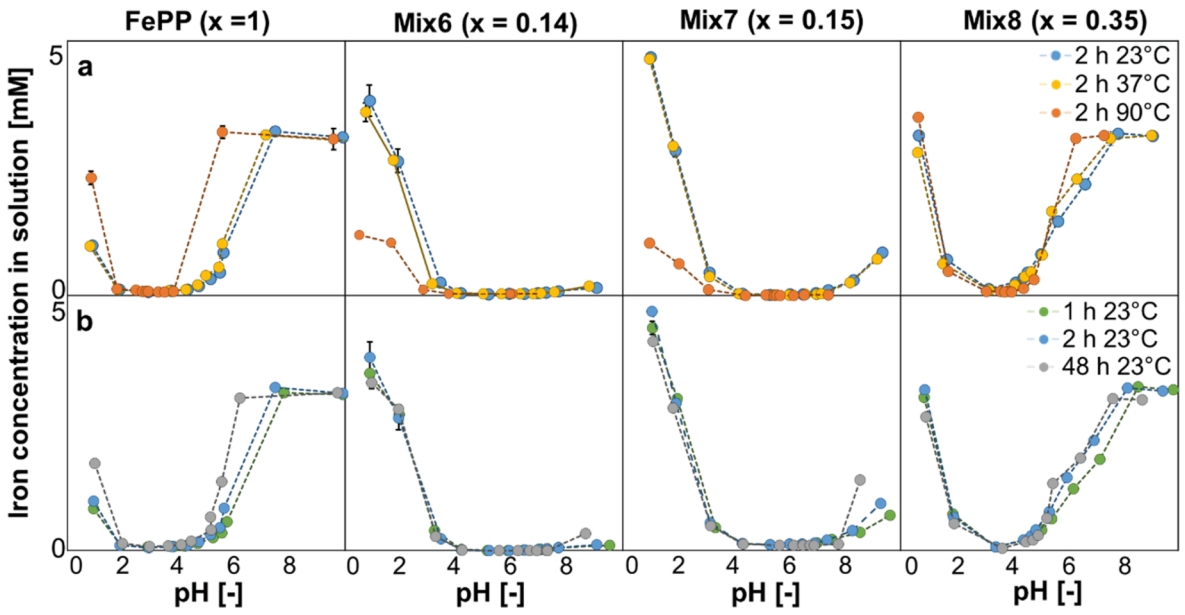

Fig. 6. Effect of (a) temperature and (b) time on pH-dependent dissolution behavior of iron in FePP and mixed Ca-Fe(III) pyrophosphate salts. (a) No significant change in iron dissolution ($p > 0.05$) was observed upon increasing the temperature from 23 °C to 37 °C over the studied pH range (1–10). Upon elevating temperature to 90 °C, an increase in dissolved iron from FePP at pH 1 and 5.5 and from Mix8 (x = 0.35) at pH ~ 7 was observed. (b) Iron dissolution pointed to no remarkable difference between iron dissolution for one and two hours of incubation. After 48 h, dissolution remained constant at all pH ranges for all salts except for FePP with a significant increase at pH < 2 and pH 5–6.

comparison between tea solutions showed that surprisingly, the discoloration induced by these salts was a non-monotonic function of their iron content. The salts Mix6 (x = 0.14), Mix7 (x = 0.15), and FePP (x = 1) resulted in visually similar discolorations in the black tea solution. However, exposing the tea solution to Mix8 (x = 0.35) increased the discoloration and resulted in the darkest tea solution compared to all other salts.

The results obtained from the UV–Vis absorbance of the tea solutions are shown in (Fig. 7**b**). The UV–Vis absorbance of the tea solutions was consistent with the discoloration (Fig. 7**a**) and showed the same non-monotonic relation between absorbance at 550 nm and iron content of the salts. Using the mixed salt Mix6 (x = 0.14) resulted in equal absorbance compared to FePP, whereas for the salt Mix7 (x = 0.15) a slightly darker color and higher absorbance was observed (**Table S1** of **Supplementary material**). After being exposed to Mix8 (x = 0.35), which had the highest iron content, the darkness of the tea solution increased significantly with an approximate 1.5-fold increase in the UV–Vis absorbance compared to pure FePP ($p < 0.05$). The discoloration induced by CaPP, shown for comparative purposes, caused slight darkening of the tea solution (lightness $L^* = 40$ for CaPP versus $L^* = 49$ for blank). It was previously reported in the literature that complexation of calcium with phenolics does not lead to a change in color (Habeych et al., 2016). However, the slight discoloration observed in the tea solution in the presence of calcium is suggested to be due to interaction and oxidation of polyphenols with calcium at elevated temperatures, which is also responsible for tea stains on the surface of teacups (Yamada, Abe, & Tanizawa, 2007). The concentration of the dissolved iron from the salts in the tea solutions was measured by ICP-AES (Fig. 7**b**). ICP-AES analysis of the pure black tea solution before the addition of any salts showed that it contained on average 2.7 ± 0.2 μg of iron per 100 ml of tea. Results showed that exposure to FePP increased the iron concentration in the tea solution to 0.25 mg per 100 ml tea. Exposure to Mix6 (x = 0.14) resulted in a 28% lower iron concentration compared to the FePP. In the case of the salt Mix7 (x = 0.15), the amount of the iron released was slightly higher (i.e., 12%) than for pure FePP. In line with the dissolution of the salts in water at pH ~ 5 (section 3.3), the dissolved iron of Mix8 was higher compared to FePP. In the tea solution tested with the salt Mix8 (x = 0.35), the dissolved iron concentration was almost 2.7 fold (0.67 mg per 100 ml tea) higher than in the tea exposed to FePP. Consequently, exposure to Mix8 (x = 0.35) resulted in significantly higher discoloration compared to the other samples ($p < 0.05$). Despite the observed discoloration of tea upon exposure to the salts, the highest measured iron concentration was only 64% of the total amount of iron added. This indicates that a considerable amount of iron was retained in the salt matrix.

Interestingly, discoloration was also observed on the surface of the insoluble proportion of the salt that was recollected as a residue upon filtration of the black tea solutions (**Fig. S5** of **Supplementary material**). All salt powders were either white or off-white before performing the reactivity experiment. The color of the residues of all iron-containing pyrophosphate salts changed to dark brown or black after being in contact with the tea solution, whereas the residue of CaPP remained white. We suggest that the iron-containing salts show darkening due to the complexation of the iron ions on the surface of the salts with the phenolics present in the black tea solution.

Although the main intention of the performed black tea experiment in this work was not to fortify tea, we used the tea solutions as a representative example to investigate the reactivity of iron from the designed mixed salts with phenolic compounds (catechins), to show the novel salts' potential for food fortification. Contrary to our expectations based on the pH-dependent dissolution assay, the mixed salts did not show noticeably less reactivity in black tea solution compared to FePP. In future experiments, the reactivity and surface interactions of the iron-containing pyrophosphate salts in the presence of phenolic compounds should be further explored using model systems of selected pure phenolic compounds to get more insight in the mechanism for phenolic-mediated discoloration by complexation and oxidation, and stability of these mixed salts in foods and during storage. Even though the mixed salts show similar reactivity compared to FePP in foods, the increased dissolution at pH 1–3 indicates that these salts likely possess improved bio-accessibility compared to FePP. To assess organoleptic properties other than color, such as flavor, the synthesis needs to be perfomed using food-grade reagents and under food-grade conditions. Moreover, the *in vivo* bioavailability of the salts, chemical stability, and the required

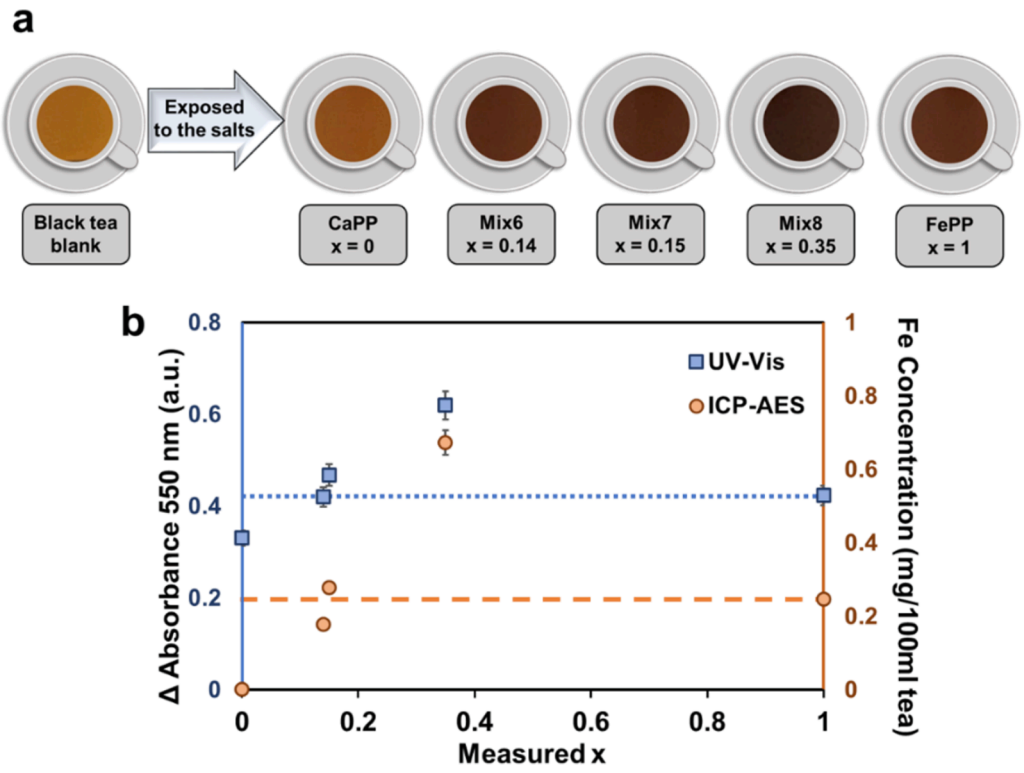

Fig. 7. The results of the reactivity assessment by exposure to a black tea solution. (a) Images show discoloration of the black tea solution after 10 min exposure to the pure salts CaPP (x = 0), FePP (x = 1), and the mixed Ca-Fe(III) pyrophosphate salts with x = 0.14, 0.15, and 0.35 compared to the blank tea solution (pH 5.13 ± 0.13). (b) Increase in absorbance of the tea solutions compared to the blank black tea solution measured at 550 nm by UV–Vis spectroscopy (blue squares, primary y-axis) and concentration of the dissolved Fe in the tea solution is determined by ICP-AES (orange circles, secondary y-axis). The horizontal lines correspond to the absorbance of the tea solution (blue, dotted) and the Fe concentration (orange, dashed) obtained for the tea solution exposed to FePP. (For interpretation of the references to color in this figure legend, the reader is referred to the web version of this article.)

safety clearance of the studied mixed pyrophosphate salts, which can be product-specific, should be addressed in future work but are beyond the scope of this manuscript.

4. Conclusion

In the present study, we report the design, synthesis, and characterization of mixed calcium and iron (III) pyrophosphate salts with the general formula $Ca_{2(1-x)}Fe_{4x}(P_2O_7)_{(1+2x)}$ ($0 \leq x \leq 1$). Mixed salts with $0.14 \leq x \leq 0.35$ were amorphous and uniform in terms of their morphology. We demonstrate for the first time the tunable pH-dependent solubility of mixed Ca-Fe(III) pyrophosphate salts. Our results indicate that the mixed salts with x = 0.14 and 0.15 have a lower iron solubility at food-relevant pH (3–7) compared to FePP. Furthermore, at gastric pH (1–3), the salts show enhanced iron dissolution with up to a fourfold increase of soluble iron compared to FePP. Assessment of the reactivity of the selected mixed Ca-Fe(III) pyrophosphate salts in a black tea solution showed that the concentration of the dissolved iron ions released from the salts was a non-monotonic function of the x-values and that none of the salts could reduce the development of discoloration compared to FePP. The present findings indicate that the mixed Ca-Fe(III) pyrophosphate salts with experimental $x \leq 0.15$ in the general formula $Ca_{2(1-x)}Fe_{4x}(P_2O_7)_{(1+2x)}$ can be potential food fortificants with tunable iron composition and dissolution behavior. The main benefit of these salts is improved bio-accessibility resulting from increased dissolution at gastric pH (1–3) compare to FePP. Furthermore, our results demonstrate that the pyrophosphate salts can be used as a carrier for iron and as a potential delivery system for dual-fortification. In future works, safety assessment of the designed mixed salts, their impact on sensorial attributes of foods, and bioavailability of the constituent iron should be further explored.

Funding Source

This research received funding from the Netherlands Organization for Scientific Research (NWO) in the framework of the Innovation Fund for Chemistry and from the Ministry of Economic Affairs in the framework of the "TKI/PPS-Toeslagregeling" (Grant 731017205).

Ethical statements

(1) This material is the authors' own original work, which has not been previously published elsewhere.
(2) The paper is not currently being considered for publication elsewhere.
(3) The paper properly credits the meaningful contributions of co-authors and co-researchers.
(4) Our research did not include human subjects or animal experiments.

CRediT authorship contribution statement

Neshat Moslehi: Conceptualization, Methodology, Investigation, Visualization, Writing – original draft. **Judith Bijlsma:** Conceptualization, Methodology, Investigation, Visualization, Writing – original draft. **Wouter J.C. de Bruijn:** Conceptualization, Supervision, Writing – review & editing. **Krassimir P. Velikov:** Conceptualization, Methodology, Supervision, Writing – review & editing. **Jean-Paul Vincken:** Conceptualization, Supervision, Writing – review & editing. **Willem K. Kegel:** Conceptualization, Supervision, Writing – review & editing.

Declaration of Competing Interest

The authors declare that they have no known competing financial interests or personal relationships that could have appeared to influence the work reported in this paper.

Acknowledgements

Hans Meeldijk from Inorganic Chemistry, Utrecht University, is thanked for TEM-EDX and HAADF-STEM measurements. Coen Mulder

from Geo-Science group of Utrecht University is thanked for ICP-AES measurements (black tea experiment). K. P. V. acknowledges the stimulating discussion with Roumen Tsekov. The authors are grateful to Arjen Reichwein, Raymond Nijveld, and Teun de Bruin of Nouryon specialty chemicals B.V. for performing the ICP-AES measurements (dissolution behavior). The graphical abstract was made with content from BioRender.com.

Appendix A. Supplementary material

Up-scaled synthesis of pure and mixed Ca-Fe(III) pyrophosphate salts (**Method S1**); Effect of calcium on the absorbance of the Fe(II)-ferrozine complex (**Fig. S1**); Iron concentration measurement by inductively coupled plasma – atomic emission spectroscopy (ICP-AES) (**Method S2**); Detailed color conversion of black tea solutions in presence of CaPP, FePP, and mixed Ca-Fe(III) pyrophosphate salts (**Table S1**); Heterogenous distribution of iron and calcium by HAADF-STEM (**Fig. S2**); Mixed Ca-Fe(III) pyrophosphate salt before and after ultrasonication treatment (**Fig. S3**); Comparison of the dissolved iron measured by the ICP-AES and the ferrozine method (**Fig. S4**); Images of the residue of pure CaPP, FePP, and mixed Ca-Fe(III) pyrophosphate salts after contact with black tea solution (**Fig. S5**). Supplementary data to this article can be found online at https://doi.org/10.1016/j.jff.2022.105066.

References

Allen, L., de Benoist, B., Dary, O., & Hurrell, R. (2006). Guidelines on Food Fortification With Micronutrients. *World Health Organization*, 341.

Ashwin, K., Pattanaik, A. K., & Howarth, G. S. (2021). Polyphenolic bioactives as an emerging group of nutraceuticals for promotion of gut health: A review. *Food Bioscience, 44*, Article 101376. https://doi.org/10.1016/J.FBIO.2021.101376

Baars, R. J., van Leeuwen, Y. M., Hendrix, Y., Velikov, K. P., Kegel, W. K., & Philipse, A. P. (2015). Morphology-controlled functional colloids by heterocoagulation of zein and nanoparticles. *Colloids and Surfaces A: Physicochemical and Engineering Aspects, 483*, 209–215. https://doi.org/10.1016/j.colsurfa.2015.04.042

Bijlsma, J., de Bruijn, W. J. C., Hageman, J. A., Goos, P., Velikov, K. P., & Vincken, J. P. (2020). Revealing the main factors and two-way interactions contributing to food discolouration caused by iron-catechol complexation. *Scientific Reports, 10*(1), 1–11. https://doi.org/10.1038/s41598-020-65171-1

Bijlsma, J., de Bruijn, W. J. C., Velikov, K. P., & Vincken, J. P. (2022). Unravelling discolouration caused by iron-flavonoid interactions: Complexation, oxidation, and formation of networks. *Food Chemistry, 370*, Article 131292. https://doi.org/10.1016/J.FOODCHEM.2021.131292

Bolade, O. P., Williams, A. B., & Benson, N. U. (2020). Green synthesis of iron-based nanomaterials for environmental remediation: A review. *Environmental Nanotechnology, Monitoring & Management, 13*, Article 100279. https://doi.org/10.1016/J.ENMM.2019.100279

Bothwell, T. H., & MacPhail, A. P. (2004). The potential role of NaFeEDTA as an iron fortificant. *International Journal for Vitamin and Nutrition Research, 74*(6), 421–434. https://doi.org/10.1024/0300-9831.74.6.421

Bovell-Benjamin, A. C., & Guinard, J. X. (2003). Novel Approaches and Application of Contemporary Sensory Evaluation Practices in Iron Fortification Programs. *Critical Reviews in Food Science and Nutrition, 43*(4), 379–400. https://doi.org/10.1080/10408690390826563

Catti, M., Ferraris, G., & Ivaldi, G. (1979). Refinement of the crystal structure of anapaite $Ca_2Fe(PO_4)_2.4H_2O$: Hydrogen bonding and relationships with the bihydrated phase. *Bulletin de Minéralogie, 102*(4), 314–318. https://doi.org/10.3406/BULMI.1979.7323

Cercamondi, C. I., Duchateau, G. S. M. J. E., Harika, R. K., Van Den Berg, R., Murray, P., Koppenol, W. P., Zeder, C., Zimmermann, M. B., & Moretti, D. (2016). Sodium pyrophosphate enhances iron bioavailability from bouillon cubes fortified with ferric pyrophosphate. *British Journal of Nutrition, 116*(3), 496–503. https://doi.org/10.1017/S0007114516002191

Díaz, J. R., De las Cagigas, A., & Rodríguez, R. (2003). Micronutrient deficiencies in developing and affluent countries. *European Journal of Clinical Nutrition, 57*, S70–S72. https://doi.org/10.1038/sj.ejcn.1601820

Dousma, J., & De Bruyn, P. L. (1976). Hydrolysis-precipitation studies of iron solutions. I. Model for hydrolysis and precipitation from Fe(III) nitrate solutions. *Journal of Colloid and Interface Science, 56*(3), 527–539. https://doi.org/10.1016/0021-9797(76)90119-3

Drenchev, N. L., Chakarova, K. K., Lagunov, O. V., Mihaylov, M. Y., Ivanova, E. Z., Strauss, I., & Hadjiivanov, K. I. (2020). In situ FTIR Spectroscopy as a Tool for Investigation of Gas/Solid Interaction: Water-Enhanced CO_2 Adsorption in UiO-66 Metal-Organic Framework. *JoVE (Journal of Visualized Experiments), 2020*(156), Article e60285. https://doi.org/10.3791/60285

Dueik, V., Chen, B. K., & Diosady, L. L. (2017). Iron-polyphenol interaction reduces iron bioavailability in fortified tea: Competing complexation to ensure iron bioavailability. *Journal of Food Quality, 2017*. https://doi.org/10.1155/2017/1805047

El Kady, A. M., Mohamed, K. R., & El-Bassyouni, G. T. (2009). Fabrication, characterization and bioactivity evaluation of calcium pyrophosphate/polymeric biocomposites. *Ceramics International, 35*(7), 2933–2942. https://doi.org/10.1016/j.ceramint.2009.03.042

Flynn, C. M., Jr. (2002). Hydrolysis of inorganic iron(III) salts. *Chemical Reviews, 84*(1), 31–41. https://doi.org/10.1021/CR00059A003

Gras, P., Rey, C., Marsan, O., Sarda, S., & Combes, C. (2013). Synthesis and Characterisation of Hydrated Calcium Pyrophosphate Phases of Biological Interest. *European Journal of Inorganic Chemistry, 2013*(34), 5886–5895. https://doi.org/10.1002/ejic.201300955

Gupta, A., Pratt, R., & Mishra, B. (2018). Physicochemical characterization of ferric pyrophosphate citrate. *BioMetals, 31*(6), 1091–1099. https://doi.org/10.1007/s10534-018-0151-1

Habeych, E., van Kogelenberg, V., Sagalowicz, L., Michel, M., & Galaffu, N. (2016). Strategies to limit colour changes when fortifying food products with iron. *Food Research International, 88*, 122–128. https://doi.org/10.1016/j.foodres.2016.05.017

Hackl, L., Zimmermann, M. B., Zeder, C., Parker, M., Johns, P. W., Hurrell, R. F., & Moretti, D. (2017). Iron Bioavailability from Ferric Pyrophosphate in Extruded Rice Cofortified with Zinc Sulfate Is Greater than When Cofortified with Zinc Oxide in a Human Stable Isotope Study. *The Journal of Nutrition, 147*(3), jn241778. https://doi.org/10.3945/jn.116.241778

Hilty, F. M., Knijnenburg, J. T. N., Teleki, A., Krumeich, F., Hurrell, R. F., Pratsinis, S. E., & Zimmermann, M. B. (2011). Incorporation of Mg and Ca into Nanostructured Fe_2O_3 Improves Fe Solubility in Dilute Acid and Sensory Characteristics in Foods. *Journal of Food Science, 76*(1), N2–N10. https://doi.org/10.1111/J.1750-3841.2010.01885.X

Hurrell, R., Nestel, Beard, & Freire. (2002). How to ensure adequate iron absorption from iron-fortified food. *Nutrition Reviews, 60*(7 Pt 2). https://doi.org/10.1301/002966402320285137.

Jiang, C. L., Wang, X. H., Parekh, B. K., & Leonard, J. W. (1998). Pyrite depression by phosphates in coal flotation. *Mining, Metallurgy & Exploration 1998 15:1, 15*(1), 1–7. https://doi.org/10.1007/BF03402779.

Joint FAO/WHO Expert Consultation: Vitamin and mineral requirements in human nutrition. (2004). World Health Organization and Food and Agriculture Organization of the United Nations.

Kosova, N. V., Rezepova, D. O., Podgornova, O. A., Slobodyuk, A. B., Petrov, S. A., & Avdeev, M. (2017). A comparative study of structure, air sensitivity and electrochemistry of sodium iron pyrophosphates $Na_{2-x}Fe_{1+x/2}P_2O_7$ (x = 0; 0.44). *Electrochimica Acta, 235*, 42–55. https://doi.org/10.1016/j.electacta.2017.03.058

Lafuente, B., Downs, R. T., Yang, H., & Jenkins, R. A. (2014). Calcioferrite with composition $(Ca_{3.94}Sr_{0.06})Mg_{1.01}(Fe_{2.93}Al_{1.07})(PO_4)_6(OH)_4{\cdot}12H_2O$. *Acta Crystallographica Section E: Structure Reports Online, 70*(3), i16–i17. https://doi.org/10.1107/S1600536814004061

Lai, Y., Liang, X., Yin, G., Yang, S., Wang, J., Zhu, H., & Yu, H. (2011). Infrared spectra of iron phosphate glasses with gadolinium oxide. *Journal of Molecular Structure, 1004*(1–3), 188–192. https://doi.org/10.1016/J.MOLSTRUC.2011.08.003

Li, Y. (2018). A review of recent research on nonequilibrium solid solution behavior in Li_XFePO_4. *Solid State Ionics, 323*, 142–150. https://doi.org/10.1016/j.ssi.2018.05.026

Luque de Castro, M. D., & Priego-Capote, F. (2007). Ultrasound-assisted crystallization (sonocrystallization). *Ultrasonics Sonochemistry, 14*(6), 717–724. https://doi.org/10.1016/j.ultsonch.2006.12.004

Marian, N. M., Giorgetti, G., Magrini, C., Capitani, G. C., Galimberti, L., Cavallo, A., Salvini, R., Vanneschi, C., & Viti, C. (2021). From hazardous asbestos containing wastes (ACW) to new secondary raw material through a new sustainable inertization process: A multimethodological mineralogical study. *Journal of Hazardous Materials, 413*, 125419. https://doi.org/10.1016/J.JHAZMAT.2021.125419

McGee, E. J. T., & Diosady, L. L. (2018a). Prevention of iron-polyphenol complex formation by chelation in black tea. *LWT - Food Science and Technology, 89*, 756–762. https://doi.org/10.1016/j.lwt.2017.11.041

McGee, E. J. T., & Diosady, L. L. (2018b). Development of Spectrophotometric Quantification Method of Iron-Polyphenol Complex in Iron-Fortified Black Tea at Relevant pH Levels. *Food Analytical Methods, 11*(6), 1645–1655. https://doi.org/10.1007/s12161-018-1147-8

Miyawaki, R., Hatert, F., Pasero, M., & Mills, S. J. (2020). IMA Commission on New Minerals, Nomenclature and Classification (CNMNC) – Newsletter 56. *European Journal of Mineralogy, 32*(4), 443–448. https://doi.org/10.5194/EJM-32-443-2020

Moretti, D., Zimmermann, M. B., Wegmüller, R., Walczyk, T., Zeder, C., & Hurrell, R. F. (2006). Iron status and food matrix strongly affect the relative bioavailability of ferric pyrophosphate in humans. *The American Journal of Clinical Nutrition, 83*(3), 632–638. https://doi.org/10.1093/ajcn.83.3.632

Ravet, N., Chouinard, Y., Magnan, J. F., Besner, S., Gauthier, M., & Armand, M. (2001). Electroactivity of natural and synthetic triphylite. *Journal of Power Sources, 97–98*, 503–507. https://doi.org/10.1016/S0378-7753(01)00727-3

Rohner, F., Ernst, F. O., Arnold, M., Hilbe, M., Biebinger, R., Ehrensperger, F., Pratsinis, S. E., Langhans, W., Hurrell, R. F., & Zimmermann, M. B. (2007). Synthesis, Characterization, and Bioavailability in Rats of Ferric Phosphate Nanoparticles 1. In *The Journal of Nutrition Nutrient Physiology, Metabolism, and Nutrient-Nutrient Interactions J. Nutr* (Vol. 137). https://academic.oup.com/jn/article/137/3/614/4664665.

Ross, A. C., Taylor, C. L., Yaktine, A. L., & Del Valle, H. B. (2011). Dietary reference intakes for adequacy: calcium and vitamin D. In *Dietary reference intakes for calcium and vitamin D* (pp. 345–402). National Academies Press: Washington, D.C. https://doi.org/10.17226/13050.

Rossi, L., Velikov, K. P., & Philipse, A. P. (2014). Colloidal iron(III) pyrophosphate particles. *Food Chemistry, 151*, 243–247. https://doi.org/10.1016/j.foodchem.2013.11.050

Saha, S., & Roy, A. (2020). Whole grain rice fortification as a solution to micronutrient deficiency: Technologies and need for more viable alternatives. *Food Chemistry, 326*, 127049. https://doi.org/10.1016/J.FOODCHEM.2020.127049

Salgueiro, M. J., & Boccio, J. (2013). Ferric pyrophosphate as an alternative iron source for food fortification. In *Handbook of Food Fortification and Health: From Concepts to Public Health Applications* (Vol. 1, pp. 91–97). Springer New York. https://doi.org/10.1007/978-1-4614-7076-2_7.

Shubham, K., Anukiruthika, T., Dutta, S., Kashyap, A. V., Moses, J. A., & Anandharamakrishnan, C. (2020). Iron deficiency anemia: A comprehensive review on iron absorption, bioavailability and emerging food fortification approaches. In *Trends in Food Science and Technology* (Vol. 99, pp. 58–75). Elsevier Ltd. https://doi.org/10.1016/j.tifs.2020.02.021.

Singh, R. K., Srivastava, M., Prasad, N. K., Awasthi, S., Dhayalan, A., & Kannan, S. (2017). Iron doped β-Tricalcium phosphate: Synthesis, characterization, hyperthermia effect, biocompatibility and mechanical evaluation. *Materials Science and Engineering C, 78*, 715–726. https://doi.org/10.1016/j.msec.2017.04.130

Srinivasu, B. Y., Mitra, G., Muralidharan, M., Srivastava, D., Pinto, J., Thankachan, P., Suresh, S., Shet, A., Rao, S., Ravikumar, G., Thomas, T. S., Kurpad, A. V., & Mandal, A. K. (2015). Beneficiary effect of nanosizing ferric pyrophosphate as food fortificant in iron deficiency anemia: Evaluation of bioavailability, toxicity and plasma biomarker. *RSC Advances, 5*(76), 61678–61687. https://doi.org/10.1039/c5ra07724a

Stookey, L. L. (1970). *Ferrozine-A New Spectrophotometric Reagent for Iron*.

Sun, Y., Zhao, L., & Teng, Y. (2020). Effect of soil type on the degradation of polychlorinated biphenyls in a pyrophosphate-chelated Fenton-like reaction. *Chemical Engineering Journal, 390*, Article 124574. https://doi.org/10.1016/J.CEJ.2020.124574

Suslick, K. S., Fang, M., & Hyeon, T. (1996). Sonochemical synthesis of iron colloids. *Journal of the American Chemical Society, 118*(47), 11960–11961. https://doi.org/10.1021/ja961807n

Swain, J. H., Newman, S. M., & Hunt, J. R. (2003). Bioavailability of elemental iron powders to rats is less than bakery-grade ferrous sulfate and predicted by iron solubility and particle surface area. *The Journal of Nutrition, 133*(11), 3546–3552. https://doi.org/10.1093/JN/133.11.3546

Tan, H. J., Dodd, J. L., & Fultz, B. (2009). Thermodynamic and kinetic stability of the solid solution phase in nanocrystalline Li_xFePO_4. *Journal of Physical Chemistry C, 113*(48), 20527–20530. https://doi.org/10.1021/jp907161z

Tian, T., Blanco, E., Smoukov, S. K., Velev, O. D., & Velikov, K. P. (2016). Dissolution behaviour of ferric pyrophosphate and its mixtures with soluble pyrophosphates: Potential strategy for increasing iron bioavailability. *Food Chemistry, 208*, 97–102. https://doi.org/10.1016/j.foodchem.2016.03.078

van Leeuwen, Y. M. (2013). *Colloidal Metal Pyrophosphates Salts Preparation, Properties and Applications, PhD Thesis*.

van Leeuwen, Y. M., Velikov, K. P., & Kegel, W. K. (2012). Morphology of colloidal metal pyrophosphate salts. *RSC Advances, 2*(6), 2534–2540. https://doi.org/10.1039/c2ra00449f

van Leeuwen, Y. M., Velikov, K. P., & Kegel, W. K. (2014). Colloidal stability and chemical reactivity of complex colloids containing Fe^{3+}. *Food Chemistry, 155*, 161–166. https://doi.org/10.1016/j.foodchem.2014.01.045

Wang, Z., Fang, C., & Mallavarapu, M. (2015). Characterization of iron-polyphenol complex nanoparticles synthesized by Sage (Salvia officinalis) leaves. *Environmental Technology and Innovation, 4*, 92–97. https://doi.org/10.1016/j.eti.2015.05.004

Wienk, K. J. H., Marx, J. J. M., & Beynen, A. C. (1999). The concept of iron bioavailability and its assessment. *European Journal of Nutrition, 38*.

Wilhelmy, R. B., Patel, R. C., & Matijević, E. (1985). Thermodynamics and Kinetics of Aqueous Ferric Phosphate Complex Formation†. *Inorganic Chemistry, 24*(20), 3290–3297. https://doi.org/10.1021/IC00214A039

Yamada, K., Abe, T., & Tanizawa, Y. (2007). Black tea stain formed on the surface of teacups and pots. Part 2–Study of the structure change caused by aging and calcium addition. *Food Chemistry, 103*(1), 8–14. https://doi.org/10.1016/j.foodchem.2006.05.069

Zheng, J. C., Ou, X., Zhang, B., Shen, C., Zhang, J. F., Ming, L., & Han, Y. D. (2014). Effects of Ni^{2+} doping on the performances of lithium iron pyrophosphate cathode material. *Journal of Power Sources, 268*, 96–105. https://doi.org/10.1016/j.jpowsour.2014.05.147

Zimmermann, M. B. (2004). The potential of encapsulated iron compounds in food fortification: A review. *International Journal for Vitamin and Nutrition Research, 74*(6), 453–461. https://doi.org/10.1024/0300-9831.74.6.453

Zimmermann, M. B., & Hilty, F. M. (2011). Nanocompounds of iron and zinc: Their potential in nutrition. *Nanoscale, 3*(6), 2390–2398. https://doi.org/10.1039/c0nr00858c

Zuidam, N. J. (2012). An industry perspective on the advantages and disadvantages of iron micronutrient delivery systems. In *Encapsulation Technologies and Delivery Systems for Food Ingredients and Nutraceuticals* (pp. 505–540). Elsevier. https://doi.org/10.1533/9780857095909.4.505.